tvst

Article

Classification of Pachychoroid on Optical Coherence Tomographic *En Face* Images Using Deep Convolutional Neural Networks

Kook Lee[1,*], Ho Ra[2,*], Jun Hyuk Lee[2], Jiwon Baek[2], and Won Ki Lee[3]

[1] Department of Ophthalmology, Seoul St. Mary's Hospital, College of Medicine, The Catholic University of Korea, Seoul, Republic of Korea
[2] Department of Ophthalmology, Bucheon St. Mary's Hospital, College of Medicine, The Catholic University of Korea, Gyeonggi-do, Republic of Korea
[3] Nune Eye Center, Seoul, Republic of Korea

Correspondence: Jiwon Baek, Department of Ophthalmology, Bucheon St. Mary's Hospital, College of Medicine, The Catholic University of Korea. #327 Sosa-ro, Wonmi-gu, Bucheon, Gyeonggi-do 14647, Republic of Korea.
e-mail: md.jiwon@gmail.com

Received: December 6, 2020
Accepted: May 11, 2021
Published: June 29, 2021

Keywords: choroid; deep learning; haller's layer; OCT; pachychoroid

Citation: Lee K, Ra H, Lee JH, Baek J, Lee WK. Classification of pachychoroid on optical coherence tomographic *en face* images using deep convolutional neural networks. Transl Vis Sci Technol. 2021;10(7):28, https://doi.org/10.1167/tvst.10.7.28

Purpose: To study the efficacy of deep convolutional neural networks (DCNNs) to differentiate pachychoroid from nonpachychoroid on *en face* optical coherence tomography (OCT) images at the large choroidal vessel.

Methods: *En face* OCT images were collected from eyes with neovascular age-related macular degeneration, polypoidal choroidal vasculopathy, and central serous chorioretinopathy. All images were prelabeled pachychoroid or nonpachychoroid based on quantitative and qualitative criteria for choroidal morphology on multimodal imaging by two retina specialists. In total, 1188 nonpachychoroid and 884 pachychoroid images were used for training (80%) and validation (20%). Accuracy for identification of pachychoroid by DCNN models was analyzed. Trained models were tested on a test set containing 79 nonpachychoroid and 93 pachychoroid images.

Results: The accuracy on the validation set was 94.1%, 93.2%, 94.7%, and 94.4% in DenseNet, GoogLeNet, ResNet50, and Inception-v3, respectively. On a test set, each model demonstrated accuracy of 80.2%, 83.1%, 89.5%, and 90.1% and an F1 score of 0.782, 0.824, 0.904, and 0.901, respectively.

Conclusions: DCNN models could classify pachychoroid and nonpachychoroid with good performance on OCT *en face* images. Automated classification of pachychoroid will be useful for tailored treatment of individual patients with exudative maculopathy.

Translational Relevance: *En face* OCT images can be used by DCNN for classification of pachychoroid.

Introduction

Pachychoroid is a condition characterized by pathologically dilated Haller vessels (i.e., pachyvessel), choriocapillaris attenuation, and choroidal vascular hyperpermeability.[1–3] These features are well observed on B-scans and *en face* images of optical coherence tomography (OCT) and indocyanine green angiography.[4,5] Recognizing pachychoroid is important in exudative maculopathies because some have distinctive features from typical age-related macular degeneration (AMD). These exudative maculopathies were often considered AMD but can now be classified into the pachychoroid category. The pattern of pachyvessel in pachychoroid diseases can best be visualized with OCT *en face* using long wavelengths such as swept-source or enhanced depth spectral-domain images.[4,6]

The spectrum of pachychoroid disease encompasses central serous chorioretinopathy (CSC), pachychoroid neovasculopathy (PNV), and thick-choroid polypoidal choroidal vasculopathy (PCV).[2,3,7] Previous studies have shown that the pattern of vessels at the choroidal large vessel layer differs between pachychoroid and nonpachychoroid eyes.[1,4,6,8–12] Vascular densities are significantly increased in diffusely distributed vessels with large diameters in pachychoroid eyes, while only focal or no

pachyvessels are observed in nonpachychoroid eyes. These findings suggest that choroidal large vessel morphology can be used to differentiate pachychoroid and nonpachychoroid eyes.

Pachychoroid and typical AMD seem to differ in clinical features, genetics, natural course, and responsiveness to treatment.[13–16] Patients with pachychoroid are usually younger.[7,14,16,17] In addition, a lower injection rate with a longer injection-free period was reported in PCV eyes with pachychoroid features.[13,18] Similar results have been reported in PNV compared to typical AMD.[19] Therefore, pachychoroid identification would be helpful in disease prognosis of a patient and in planning tailored treatment options and follow-up intervals.

As diagnosis of retinal diseases depends largely on imaging, artificial intelligence (AI), especially its subclassification deep learning, has been actively applied in many areas of retina-associated disease, including diabetic retinopathy and AMD.[20–22] Deep convolutional neural networks (DCNN) have been applied to achieve automated grading of AMD using color fundus images[20] to detect specific lesions and subtypes of AMD, as well as in decision making for treatment.[23–25] In the current study, we investigated the performance of DCNN models for detection of pachychoroid using *en face* OCT images at the choroidal large vessel layer level to investigate the potential of automatic classification of pachychoroid. As this is the first study to train DCNN models using *en face* OCT images, the results of the current study will also provide details of the DCNN models that could be useful in future studies using *en face* OCT images.

Materials and Methods

The study was approved by the Institutional Review Board of Seoul and Bucheon St. Mary's Hospital (HC19RESI0086 and HC21RASI0007), which waived the need for written informed consent because of the study's retrospective design. The study was conducted in accordance with the tenets of the Declaration of Helsinki.

Subjects

En face OCT images of patients with exudative macular diseases, including typical AMD, PCV, PNV, and CSC, were collected from consecutive patients who visited Seoul St. Mary's Hospital (The Catholic University of Korea, Republic of Korea) between April 2016 and July 2020. All patients underwent high-definition OCT (DRI OCT Triton; Topcon Corporation, Tokyo, Japan) with enhanced depth imaging, fluorescent angiography (Optos California P200DTx; Optos, Dunfermline, United Kingdom), and indocyanine green angiography (ICGA; Optos California P200DTx) at baseline to confirm the diagnosis.

All images were prelabeled as pachychoroid or nonpachychoroid. Confirmation of pachychoroid strictly followed the quantitative and qualitative definition described below by two retina specialists to avoid controversies. The criteria were based on thorough review of previous publications and comprised[7]: (1) subfoveal choroidal thickness (SFCT) $\geq$ 300 µm and (2) presence of attenuation of the inner choroid with dilated choroidal vessels (pachyvessel) under the diseased area on OCT B-scans. (3) Presence of pachydrusen on fundus photography and OCT and choroidal vascular hyperpermeability on ICGA were the optional features used to confirm pachychoroid. We specified the quantitative value of SFCT and utilized multimodal images in the definition of pachychoroid to minimize the ambiguity of distinguishing pachychoroid from nonpachychoroid.

The exclusion criteria for this study were as follows: (1) choroidal neovascularization other than AMD (e.g., punctate inner choroidopathy, vitelliform dystrophy); (2) history of previous treatment or scar at the retina (e.g., photodynamic therapy, laser photocoagulation, intraocular injections, periocular injections, and systemic injections); (3) high myopia (>-6.00 diopters or axial length $>$ 26 mm); (4) poor image quality (signal strength index $<$ 40); and (5) large subretinal/preretinal hemorrhage or pigment epithelial detachment that could obscure the choroidal vascular image.

Image Preparation, Model Training, and Performance Metrics

Assessment of choroidal morphology was largely based on our previous studies.[4,13] Volume data of the posterior pole were acquired over a 12 $\times$ 9 mm^2 area containing 512 $\times$ 256 A-scans using OCT. *En face* image acquisition was subjected to automated segmentation and topology normalization using IMAGEnet6 software (version 1.19.11030; Topcon Corporation, Tokyo, Japan), with the Bruch's membrane used as a reference plane for "flattening" operation. *En face* images of choroidal large vessel layer used in this study were obtained at 50% of the total choroidal thickness for analysis of the large choroidal vessel layer. All images were saved as JPEG files.

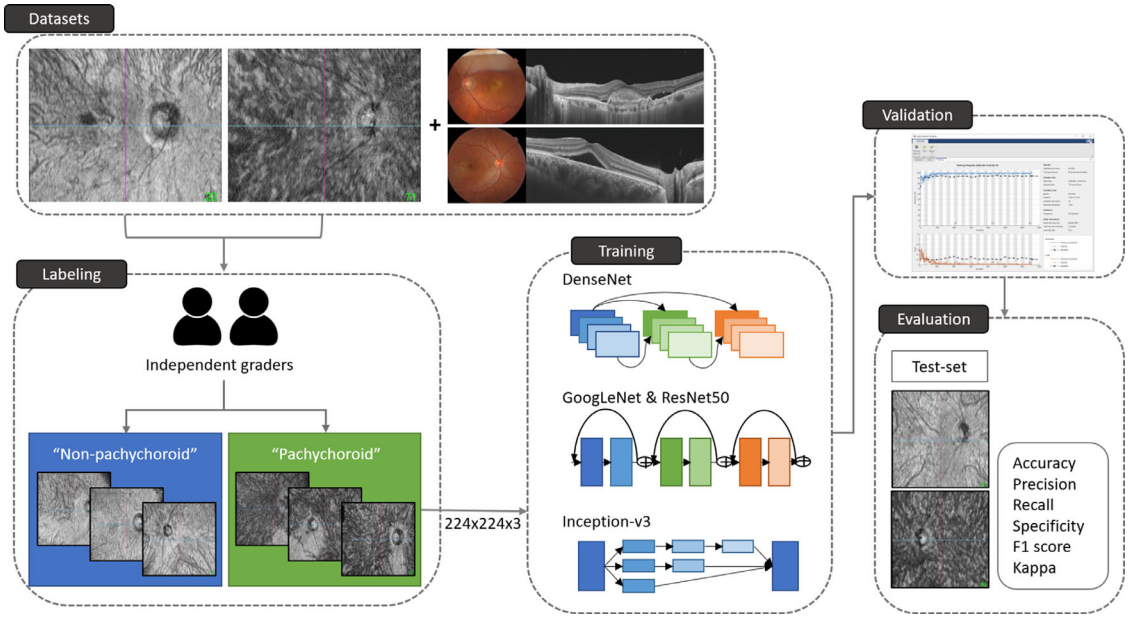

Figure 1. Training, internal validation, and external validation of deep convolutional neural network (DCNN) models. *En face* optical coherence tomographic (OCT) images were obtained at the level of total choroidal thickness for analysis of the large choroidal vessel layer. The images were labeled either "pachychoroid" or "nonpachychoroid" by two independent graders. Each *en face* OCT image was scaled to 224 × 224 × 3 pixels for DCNN training and trained using DenseNet, GoogLeNet, ResNet50, and Inception-v3 architectures. From the dataset, 80% of the images were used for training, and the remaining 20% was used for validation. Trained DCNN models were externally validated using a test set.

Training and validation of DCNN models were performed using MATLAB R2020a (MathWorks, Inc., Natick, MA, USA). Among various pretrained DCNN architectures, this study included DenseNet, GoogLeNet, ResNet50, and Inception-v3 for transfer learning. DCNN is a neural network that can process three-dimentional data of color images and composed of convolution layer and pooling layer. A brief description for each DCNN architecture used in this study follows: (1) DenseNet utilizes dense connections between layers, through Dense Blocks, all layers with matching feature-map sizes are connected directly with each other; (2) GoogLeNet is a 22-layer CNN which is a variant of the Inception, in which stack modules or blocks within which are convolutional layers; (3) ResNet50 also stacks blocks and consists of five stages each with a convolution and Identity block; (4) Inception-v3 is an architecture from the Inception family with several improvements (Fig. 1). Selection of DCNN architectures was based on the top-5 error rate reported previously in image classification and application in ophthalmologic images.[26,27]

During the training process, each *en face* OCT image was scaled to 224 × 224 × 3 pixels. The input images were labeled as either "pachychoroid" or "nonpachychoroid" by two independent graders experienced in retinal imaging. In total, 1267 nonpachychoroid and 977 pachychoroid images were collected. Randomly selected 79 nonpachychoroid and 93 pachychoroid images were used as a test set. Rule of thumb was not applied in distribution of test set to use more data on model training and validation. The rest of the images were trained with 80% of the dataset, which was randomly selected: 950 nonpachychoroid and 707 pachychoroid images. The remaining 20% was used as the validation set: 238 nonpachychoroid and 177 pachychoroid images. The performance of trained models was tested on a test set.

All experiments were conducted on a computer equipped with NVIDIA RTX 2060 and Intel i7 CPUs. Each model was trained for 30 epochs with a maximum of 1320 iterations. The performance of each model was evaluated for accuracy, precision, recall (sensitivity), specificity, F1 score, and kappa score.

Statistics

Statistical analysis was performed using a commercial program (Statistical Package for the Social Sciences version 22.0.1 for Windows; IBM Corp., Armonk, NY, USA). Independent *t*-test was used to compare demographics between groups, and the chi-square test was used to compare categorical variables. Accuracy, precision, recall, specificity, and F1 score were

Table 1. Characteristics of Each Dataset

	Nonpachychoroid	Pachychoroid	*P*-Value
Dataset for training and validation			
Image numbers (*n*)	1188	884	
Age, years (mean ± SD)	73.78 ± 8.83	61.59 ± 12.24	<0.001
Gender (% male)	50.19%	70.49%	<0.001
Subfoveal choroidal thickness, µm (mean ± SD)	135.22 ± 64.23	405.40 ± 93.86	<0.001
Diagnosis			
CSC/PNV/PCV/AMD (*n*, %)	0(0)/0(0)/332(28)/855(72)	335(38)/214(24)/335(38)/0(0)	
Test set			
Image numbers	79	93	
Age, years (mean ± SD)	73.90 ± 10.44	59.62 ± 12.5	<0.001
Gender (% male)	41.94%	70.76%	0.001
Subfoveal choroidal thickness, µm (mean ± SD)	150.27 ± 76.52	417.46 ± 106.43	<0.001
Diagnosis			
CSC/PNV/PCV/AMD (*n*, %)	0(0)/0(0)/22(28)/57(72)	35(38)/23(24)/35(38)/0	
P-values for comparison between dataset and test set			
Age	0.93	0.208	
Gender	0.211	0.963	
Subfoveal choroidal thickness, µm	0.144	0.248	

SD: standard deviation; CSC: central serous chorioretinopathy; PNV: pachychoroid neovasculopathy; PCV: polypoidal choroidal vasculopathy; AMD: age-related macular degeneration.

calculated for each model. The kappa score mean and standard deviation (SD) were used to determine the agreement between truth and each model.

Results

Characteristics of the Subjects

In total, 370 images of CSC, 237 images of PNV, 370 images of PCV, and 912 images of typical AMD were used for training/validation and test. For the dataset used in training and validation, the mean age in the nonpachychoroid and pachychoroid group was 73.78 ± 8.83 and 61.59 ± 12.24, respectively ($P < 0.001$). Proportion of male was 50.19% and 70.49%, respectively ($P < 0.001$). For the test set, the mean age was 73.90 ± 10.44 and 59.62 ± 12.5 ($P < 0.001$) and the male percentage was 41.94% and 70.76% ($P = 0.001$) for nonpachychoroid and pachychoroid, respectively. No statistical difference was observed in mean age, sex distribution, or subfoveal choroidal thickness between the dataset and test set (all $P \geq 0.144$). Clinical characteristics of the subjects are summarized in Table 1.

Performance of the DCNN Models

The final accuracy on the validation set was 94.1%, 93.2%, 94.7%, and 94.4% in DenseNet, GoogLeNet, ResNet50, and Inception-v3, respectively (Fig. 2). The time spent in model training was 171, 9, 21, and 37 minutes, respectively.

In a test set, the models demonstrated 80.2%, 83.1%, 89.5%, and 90.1% accuracy, respectively. The precision of the models was 0.9683, 0.9444, 0.8947, and 0.9872 and recall was 0.6559, 0.7312, 0.9140, and 0.8280, respectively. The F1 score of each model was 0.7821, 0.8242, 0.9043, and 0.9006, respectively. The accuracy, precision, recall, specificity, F1 score, and kappa values of each model are summarized in Table 2.

Analysis of Prediction Errors of DCNN Models

In the test set, one nonpachychoroid image was misclassified as pachychoroid, and 11 pachychoroid images were misclassified as nonpachychoroid by all four models. The images of the nonpachychoroid eye that was misclassified as pachychoroid were from a 64-year-old female with PCV (Fig. 3). Although the image was labeled as nonpachychoroid due to a subfoveal choroidal thickness of 219 µm, OCT B-scans of the eye revealed dilated vessels under the lesion, and *en face* OCT revealed increased vascular density with diffuse distribution of dilated large vessels. For pachychoroid eyes that were misclassified as nonpachychoroid, all eyes were diagnosed with PCV, and the mean subfoveal choroidal thickness was 303.82 ± 5.46

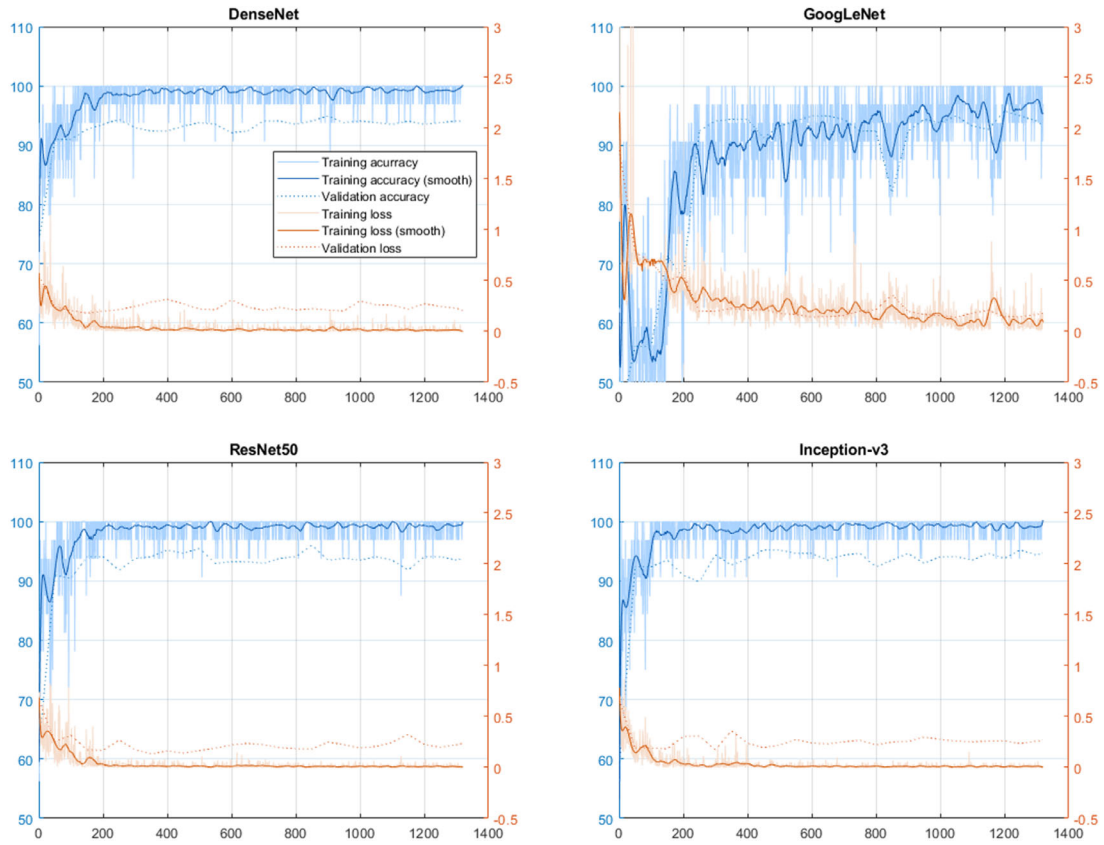

Figure 2. Internal validation performances of the models. The final accuracy of the 20% validation set was 94.1%, 93.2%, 94.7%, and 94.4% in DenseNet, GoogLeNet, ResNet50, and Inception-v3, respectively.

Table 2. Classification Performance of the Deep Convolutional Neural Network Models

	DenseNet	GoogLeNet	ResNet50	Inception-v3
Accuracy	0.8023	0.8314	0.8953	0.9012
Precision	0.9683	0.9444	0.8947	0.9872
Recall (sensitivity)	0.6559	0.7312	0.9140	0.8280
Specificity	0.9747	0.9494	0.8734	0.9873
F1 score	0.7821	0.8242	0.9043	0.9006
Kappa-mean	0.6130	0.6670	0.7920	0.8040
Kappa-SD	0.0560	0.0550	0.0450	0.0440

SD: standard deviation, F1 score = 2× (precision × recall)/(precision + recall).

(range: 300–315 µm). Figure 4 shows a representative case of a misclassified pachychoroid image.

Discussion

Pachychoroid should be distinguished from other causes of exudative maculopathy, especially typical AMD, because these two conditions differ in clinical features, genetics, natural course, and responsiveness to treatment.[13–16] In the current study, we evaluated the performance of several DCNN models trained to classify nonpachychoroid and pachychoroid using *en face* OCT images. The results demonstrated that the DCNN model could identify pachychoroid eyes with good performance, and certain DCNN architectures showed better performance than others. Analysis of errors in classification revealed that most occurred in PCV eyes with equivocal features.

Description of vascular patterns at the choroidal large vessel level was initiated by Dansingani et al.[1] They demonstrated that diseases of pachychoroid entities share morphologic findings in the choroid, including increased thickness and dilated

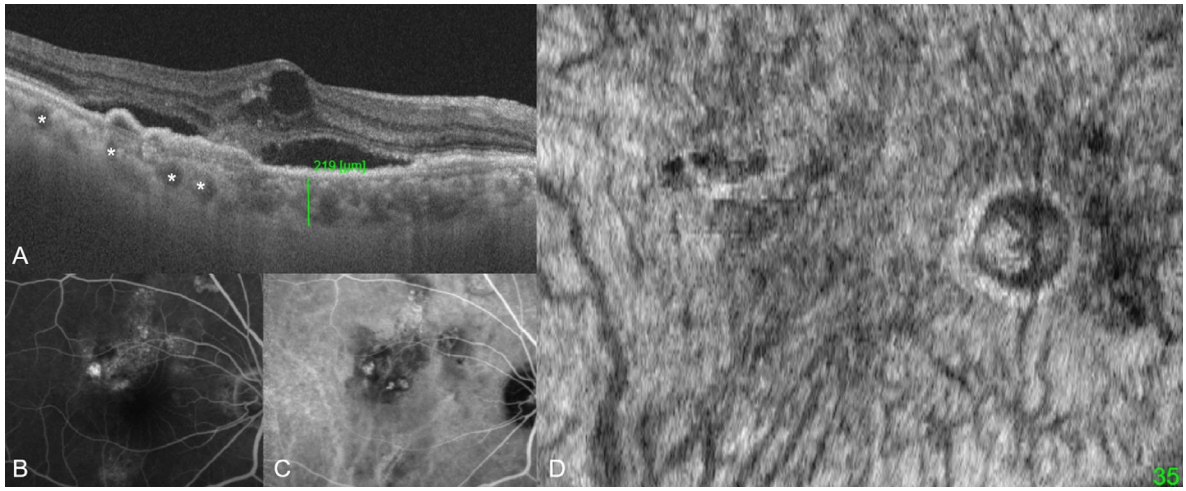

Figure 3. A representative case of a nonpachychoroid eye misclassified as pachychoroid. A. Optical coherence tomography (OCT) B-scan demonstrates a subfoveal choroidal thickness of 219 µm, but dilated Haller's vessels are seen under the lesion (asterisks). B & C. Indocyanine green angiography and fluorescein angiography reveal polypoidal lesion and leakage, confirming the diagnosis of polypoidal choroidal vasculopathy. D. *En face* OCT shows increased vascular density with diffuse distribution of Haller's vessels, which might have caused misclassification of this eye as pachychoroid.

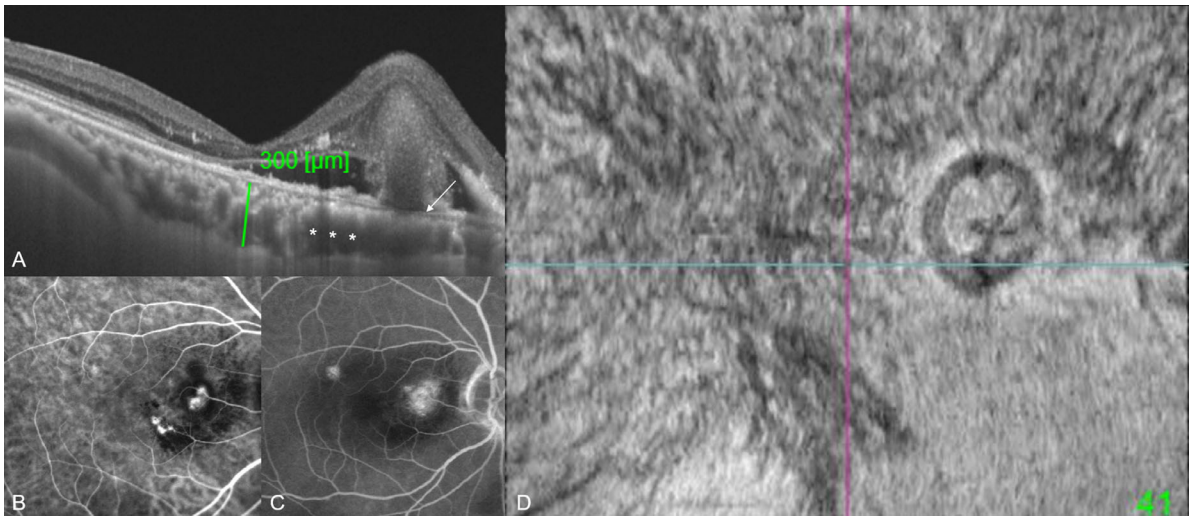

Figure 4. A representative case of a pachychoroid eye misclassified as nonpachychoroid. A. Optical coherence tomography (OCT) B-scan demonstrates subfoveal choroidal thickness of 300 µm, diffusely dilated Haller's vessels (asterisks), and attenuation of choriocapillaris + Sattler's layer under the lesion (arrow). B & C. Indocyanine green angiography and fluorescein angiography reveal polypoidal lesion and leakage, confirming the diagnosis of polypoidal choroidal vasculopathy. D. Although *en face* OCT shows diffuse distribution of Haller's vessels, the diameter of the vessels does not appear increased, which might have caused misclassification of this eye as nonpachychoroid.

outer choroidal vessels seen on OCT *en face*. Numerous studies have confirmed the peculiar morphology of the choroidal vasculature of pachychoroid eyes, especially based on *en face* OCT images.[1,4,6,28–30] Ng et al.[6] revealed that different exudative maculopathies show distinctive choroidal vasculature morphology and can be classified accordingly. Vascular density had a greater diffuse pattern of dilated vessels in pachychoroid eyes compared to nonpachychoroid AMD eyes in quantitative analysis.[4,30] These morphologic differences can serve as features that could distinguish pachychoroid from nonpachychoroid eyes for DCNNs.

In this study, DCNN architectures of DenseNet, GoogLeNet, ResNet50, and Inception-v3 were trained using *en face* OCT images that represent features of the choroidal large vessel level in each disease. The results revealed an accuracy of 80.2% to 90.1% with the independent test set. In our previous study, we demonstrated the feasibility of an auto-AI platform

trained with ultrawidefield ICGA in identification of pachychoroid.[11] The precision and recall of the model was up to 89.19%. DCNN models trained with *en face* OCT images in the current study showed comparable results in terms of precision compared to the auto-AI platform models trained using ultrawidefield ICGA images. The model trained with ResNet50 in this study revealed better performance in both precision and recall.

There was some difference in performance of models trained with different DCNN architectures. The F1 scores of ResNet50 and Inception-v3 were higher than those of DenseNet and GoogLeNet. This may be due to their inherent capacity for image classification, as demonstrated with lower error rates in previous ImageNet Large Scale Visual Recognition Challenges[27], or the feasibility of the architecture for *en face* OCT images. The performances of ResNet50 and Inception-v3 were not only better, but the time consumed in training was fairly short relative to that of DenseNet. This result may assist in selection of DCNN architecture in training *en face* OCT images for future studies.

For all DCNN models, the final accuracies for validation were higher compared to the accuracies yielded from the test set. This suggests the possibility of overfitting the models. To maximize the size of the training data, we included images from both eyes if the disease was bilateral, and this might have caused differences in internal validation of datasets and external validation using test sets. Nonetheless, the DCNN models demonstrated good performance, as demonstrated by high precision, recall, specificity, F1 score, and kappa score on external validation, especially with ResNet50 and Inception-v3.

Analysis of the prediction errors revealed that misclassifications are likely to occur in equivocal cases, and a large proportion of these equivocal cases may contain PCV. Subfoveal choroidal thickness shows bimodal distribution with two peaks around 170 µm and 360 µm, and this suggests inhomogeneity of the disease in terms of choroidal morphology.[17] Further studies are needed to support this hypothesis by showing different characteristics of PCV eyes with thin and thick choroid.[4,6,13,15] Most of the misclassification occurred in eyes with a subfoveal choroidal thickness between 300 and 315 µm. This can be interpreted as decreased capacity of the model to differentiate eyes in an overlapping range between nonpachychoroid and pachychoroid. Alternatively, it may also be explained by the possible existence of PCV entities with overlapping characteristics of thin and thick choroid, a hypothesis that requires further studies for support.

Several limitations of this study should be considered. First, there might be a selection bias caused by omitting images with poor quality or other blocking materials. Eyes with large pigment epithelial detachment or hemorrhage should be treated carefully, but DCNN models trained in this study cannot distinguish such eyes. Second, the definition of pachychoroid may be controversial. Borrelli et al.[31] reported that15.4% of neovascular AMD subjects were re-evaluated as pachychoroid. We minimized the controversy by specifying the quantitative value of SFCT and exploring multimodal images by two graders in setting the ground truth. Nonetheless, this can be a clear limitation of the current study since there can be overlap of SFCT between pachychoroid and nonpachychoroid eyes.[32] Third, there was a significant difference in age and sex distribution between pachychoroid and nonpachychoroid eyes both in the dataset and test set. However, we believe this will not significantly affect clinical application of the models since younger age and male prominence are well-established features of pachychoroid and also should be observed in real life.[6,17] Further research involving *en face* images from many OCT machines and more retinal specialists are warranted to validate the results of the current investigation.

In conclusion, DCNN models could distinguish pachychoroid from nonpachychoroid with good performance on OCT *en face* images. To the best of our knowledge, this is the first AI article that has dealt with *en face* OCT images and implies that OCT images of not only B-scans, but also *en face* scans can be used in automatizing disease classification. Furthermore, automated classification of pachychoroid will improve treatment of patients with exudative maculopathies by assisting in tailored treatment of each diseased eye.

Acknowledgments

Supported by the Institute of Clinical Medicine Research of Bucheon St. Mary's Hospital, Research Fund, 2020 and a grant from the Korea Health Technology R&D Project through the Korea Health Industry Development Institute, funded by the Ministry of Health and Welfare, Republic of Korea (grant no: HI17C2012030018).

Contributions were as follows: H.R., preparation of data and data analysis; N.Y.K., preparation of data; J.H.L., collection of data and data analysis; K.L., data analysis; J.B., conception and design of the study, writing manuscript text, preparing figures, collection and assembly of data, data analysis and interpretation,

and supervision; W.K.L: supervision. All authors reviewed the manuscript.

Disclosure: **K. Lee,** None; **H. Ra,** None; **J.H. Lee,** None; **J. Baek,** None; **W.K. Lee,** None

[*] KL and HR contributed equally to this work.

References

1. Dansingani KK, Balaratnasingam C, Naysan J, Freund KB. En face imaging of pachychoroid spectrum disorders with swept-source optical coherence tomography. *Retina*. 2016;36:499–516.
2. Pang CE, Freund KB. Pachychoroid neovasculopathy. *Retina*. 2015;35:1–9.
3. Warrow DJ, Hoang QV, Freund KB. Pachychoroid pigment epitheliopathy. *Retina*. 2013;33:1659–1672.
4. Baek J, Lee JH, Jung BJ, Kook L, Lee WK. Morphologic features of large choroidal vessel layer: age-related macular degeneration, polypoidal choroidal vasculopathy, and central serous chorioretinopathy. *Graefes Arch Clin Exp Ophthalmol*. 2018;256:2309–2317.
5. Spaide RF, Hall L, Haas A, et al. Indocyanine green videoangiography of older patients with central serous chorioretinopathy. *Retina*. 1996;16:203–213.
6. Ng DS, Bakthavatsalam M, Lai FH, et al. Classification of exudative age-related macular degeneration with pachyvessels on en face swept-source optical coherence tomography. *Invest Ophthalmol Vis Sci*. 2017;58:1054–1062.
7. Yanagi Y. Pachychoroid disease: a new perspective on exudative maculopathy. *Jpn J Ophthalmol*. 2020;64(4):323–337.
8. Kuroda Y, Ooto S, Yamashiro K, et al. Increased choroidal vascularity in central serous chorioretinopathy quantified using swept-source optical coherence tomography. *Am J Ophthalmol*. 2016;169:199–207.
9. Sasahara M, Tsujikawa A, Musashi K, et al. Polypoidal choroidal vasculopathy with choroidal vascular hyperpermeability. *Am J Ophthalmol*. 2006;142:601–607.
10. Hirahara S, Yasukawa T, Kominami A, Nozaki M, Ogura Y. Densitometry of choroidal vessels in eyes with and without central serous chorioretinopathy by wide-field indocyanine green angiography. *Am J Ophthalmol*. 2016;166:103–111.
11. Kim IK, Lee K, Park JH, Baek J, Lee WK. Classification of pachychoroid disease on ultrawidefield indocyanine green angiography using automachine learning platform. *Br J Ophthalmol*. 2021;105(6):856–861.
12. Pang CE, Shah VP, Sarraf D, Freund KB. Ultrawidefield imaging with autofluorescence and indocyanine green angiography in central serous chorioretinopathy. *Am J Ophthalmol*. 2014;158:362–371.e362.
13. Baek J, Lee JH, Lee K, Chung BJ, Lee WK. Clinical outcome of polypoidal choroidal vasculopathy/aneurysmal type 1 neovascularization according to choroidal vascular morphology. *Retina*. 2020;40(11):2166–2174.
14. Chang YC, Cheng CK. Difference between pachychoroid and nonpachychoroid polypoidal choroidal vasculopathy and their response to anti-vascular endothelial growth factor therapy. *Retina*. 2020;40(7):1403–1411.
15. Forte R, Coscas F, Serra R, Cabral D, Colantuono D, Souied EH. Long-term follow-up of quiescent choroidal neovascularisation associated with age-related macular degeneration or pachychoroid disease. *Br J Ophthalmol*. 2020;104(8):1057–1063.
16. Miyake M, Ooto S, Yamashiro K, et al. Pachychoroid neovasculopathy and age-related macular degeneration. *Sci Rep*. 2015;5:16204.
17. Lee WK, Baek J, Dansingani KK, Lee JH, Freund KB. Choroidal morphology in eyes with polypoidal choroidal vasculopathy and normal or subnormal subfoveal choroidal thickness. *Retina*. 2016;36(Suppl 1):S73–S82.
18. Morimoto M, Matsumoto H, Mimura K, Akiyama H. Two-year results of a treat-and-extend regimen with aflibercept for polypoidal choroidal vasculopathy. *Graefes Arch Clin Exp Ophthalmol*. 2017;255:1891–1897.
19. Matsumoto H, Hiroe T, Morimoto M, Mimura K, Ito A, Akiyama H. Efficacy of treat-and-extend regimen with aflibercept for pachychoroid neovasculopathy and type 1 neovascular age-related macular degeneration. *Jpn J Ophthalmol*. 2018;62:144–150.
20. Burlina PM, Joshi N, Pekala M, Pacheco KD, Freund DE, Bressler NM. Automated grading of age-related macular degeneration from color fundus images using deep convolutional neural networks. *JAMA Ophthalmol*. 2017;135:1170–1176.
21. Gargeya R, Leng T. Automated identification of diabetic retinopathy using deep learning. *Ophthalmology*. 2017;124:962–969.
22. Ting DSW, Cheung CY-L, Lim G, et al. Development and validation of a deep learning system for

diabetic retinopathy and related eye diseases using retinal images from multiethnic populations with diabetes. *JAMA*. 2017;318:2211–2223.
23. Yang HL, Kim JJ, Kim JH, et al. Weakly supervised lesion localization for age-related macular degeneration detection using optical coherence tomography images. *PLoS One*. 2019;14: e0215076.
24. Treder M, Lauermann JL, Eter N. Automated detection of exudative age-related macular degeneration in spectral domain optical coherence tomography using deep learning. *Graefes Arch Clin Exp Ophthalmol*. 2018;256:259–265.
25. Hwang DK, Hsu CC, Chang KJ, et al. Artificial intelligence-based decision-making for age-related macular degeneration. *Theranostics*. 2019;9:232–245.
26. Ting DSW, Pasquale LR, Peng L, et al. Artificial intelligence and deep learning in ophthalmology. *Br J Ophthalmol*. 2019;103:167–175.
27. Véstias MP. A survey of convolutional neural networks on edge with reconfigurable computing. *Algorithms*. 2019;12(8):154.
28. Lee WJ, Lee JW, Park SH, Lee BR. En face choroidal vascular feature imaging in acute and chronic central serous chorioretinopathy using swept source optical coherence tomography. *Br J Ophthalmol*. 2017;101:580–586.
29. Agrawal R, Chhablani J, Tan KA, Shah S, Sarvaiya C, Banker A. Choroidal vascularity index in central serous chorioretinopathy. *Retina*. 2016;36:1646–1651.
30. Wong RL, Singh SR, Rasheed MA, et al. En-face choroidal vascularity in central serous chorioretinopathy. *Eur J Ophthalmol*. 2021;31(2):536–542.
31. Borrelli E, Battista M, Gelormini F, et al. Rate of misdiagnosis and clinical usefulness of the correct diagnosis in exudative neovascular maculopathy secondary to AMD versus pachychoroid disease. *Sci Rep*. 2020;10:20344.
32. Hosoda Y, Miyake M, Yamashiro K, et al. Deep phenotype unsupervised machine learning revealed the significance of pachychoroid features in etiology and visual prognosis of age-related macular degeneration. *Sci Rep*. 2020;10:18423.